Optical and Quantum Electronics (2024) 56:786
https://doi.org/10.1007/s11082-024-06650-x

Nanocomposite film combines polyvinyl alcohol and iron oxide capped in silica for optical applications

T. S. Soliman[1,2] · A. Khalid[3] · Mohamed Taha[4] · R. M. Ahmed[5]

Received: 5 November 2023 / Accepted: 12 February 2024

Abstract
Solution-casting was used to create films of polyvinyl alcohol (PVA) nanocomposite containing different concentrations of $Fe_3O_4@SiO_2$ nanoparticles (NPs). The co-precipitation technique was used to synthesize $Fe_3O_4@SiO_2$ NPs. $Fe_3O_4@SiO_2$ impact on the PVA structure was investigated via X-ray diffraction (XRD), optical microscope, and Fourier transform-infrared (FT-IR) techniques. XRD reveals the destruction of the PVA semi-crystallinity with the $Fe_3O_4@SiO_2$ additive. FT-IR analysis supported hydrogen bond formation between PVA molecules and the $Fe_3O_4@SiO_2$ surface. The UV–visible spectrophotometer was used to investigate the optical parameters. The optical bandgap decreased with increasing the $Fe_3O_4@SiO_2$ concentration in the PVA matrix. Based on the optical bandgap, the theoretical linear refractive index (n) was deduced with theoretical models. The enhancement in the nonlinear refractive index and nonlinear optical susceptibility with the $Fe_3O_4@SiO_2$ additive to the PVA matrix makes it a possible material for nonlinear optical devices.

Keywords $Fe_3O_4@SiO_2$ nanoparticles · Polyvinyl alcohol · Refractive index · UV–visible spectrophotometer · Wemple-DiDominco model

✉ T. S. Soliman
tarek.attia@fsc.bu.edu.eg

A. Khalid
ahmed.abdelkhalik@feng.bu.edu.eg

Mohamed Taha
prof_mtm@yahoo.com

R. M. Ahmed
rania.7.8.2016@gmail.com

[1] Institute of Natural Sciences and Mathematics, Ural Federal University, Ekaterinburg, Russian Federation 620000

[2] Physics Department, Faculty of Science, Benha University, Benha 13518, Egypt

[3] Department of Basic Engineering Sciences, Faculty of Engineering (Shoubra), Benha University, Benha, Egypt

[4] Nano Gate, Hodashaarawy, Al Abageyah, El Mukkatam, 9254, Cairo 43511, Egypt

[5] Physics Department, Faculty of Science, Zagazig University, Zagazig 44519, Egypt

Published online: 25 March 2024

1 Introduction

The new industrial innovations that use polymer nanocomposites are considered among the most promising materials for organic electronic applications. Various polymer matrices were used as host materials for different nanofillers to enhance their performance to be nominated for various industrial applications (Nangia et al. 2019).

One of the well-known polymer materials, Polyvinyl alcohol (PVA), is used in practical applications like gas sensors, solar cells, optical lenses, and optoelectronic component devices (Badapanda et al. 2013; Ismail et al. 2022; Aziz et al. 2019). This relates to their unique properties like good film fabrications and mechanical, dielectric, and optical properties (Ali 2020; Heiba et al. 2022; Selvi et al. 2020). Furthermore, the hydrogen bonding between the PVA molecules and any fillers depends on the hydroxyl groups that characterize the PVA matrix (Aziz et al. 2019; Heiba et al. 2022).

Magnetic iron oxide (Fe_3O_4) nanoparticles (NPs) are utilized in different applications like solar thermal energy harvesting, electrochemical biosensors, heavy metals absorbers, and drug delivery systems (Radoń et al. 2017; Silva et al. 2013; Nikmah et al. 2019a). This is due to their compatibility, biodegradability, a wide range of photon absorption cross-section, and superparamagnetic properties (Radoń et al. 2017; Silva et al. 2013; Nabil et al. 2022). Nowadays, most researchers focus on enhancing their performance by changing their size and shape to expand their possible usage in various applications. Fe_3O_4 in the nanoscale exhibits a strong absorption at the surface. This makes it oxidized easily and reduces its potential applications. One of the most promising methods to reduce this drawback is by covering Fe_3O_4 NPs with a shell from outside, like TiO_2 and SiO_2. Silica (SiO_2) has characteristics like a high ratio of surface-to-volume, porous nature, and less reflection of light that could surround Fe_3O_4 NPs and form silanol groups (Si–OH) on their surfaces (Divya et al. 2022; Kang et al. 2019). This enables various hybrid nanostructured compounds for use in various fields. Through the silanol groups on the Fe_3O_4@SiO_2 surface and -OH groups of the PVA matrix, the interaction and connection between the PVA molecules and the Fe_3O_4@SiO_2 NPs is easy to happen and form nanocomposite material with a new structure and novel properties.

Recently, PVA was used as a host matrix for magnetic nanoparticles (for example, Fe (Soliman and Vshivkov 2019), Fe_2O_3 (Donya et al. 2020), Fe_3O_4 (Sabarudin et al. 2017; Jannah et al. 2017; Ghanbari et al. 2014), etc.), and their properties have been investigated. Fe_3O_4 NPs have a large surface volume ratio and high chemical activity on their surface, which causes their properties and dispersibility to decline (Sajid et al. 2023; Nikmah et al. 2019b). While encapsulating Fe_3O_4 by SiO_2 modifies its functionalization (Sajid et al. 2023; Nikmah et al. 2019b). To our knowledge, no published report on using Fe_3O_4@SiO_2 NPs as a filler in the PVA matrix. Towards enhancing polymer properties to be a promising material for optical and industrial applications, the present work aims to fabricate a novel nanocomposite system from a PVA as a host matrix for the Fe_3O_4@SiO_2 NPs as a filler. The characterization was done with the help of XRD, FTIR, and SEM techniques. The optical parameters were investigated using the absorption data collected from the UV–visible spectrophotometer.

2 Experimental

2.1 Preparation of Fe_3O_4@SiO_2 NPs and PVA-Fe_3O_4@SiO_2 films

Fe_3O_4 NPs were initially synthesized using the co-precipitation method, and subsequently, the Fe_3O_4@SiO_2 NPs were produced using a modified Stöber procedure, as previously described (Khalid et al. 2023). At 70 °C, dissolve 4.0 g of PVA in 80 ml of distilled-water (1.0 g/20 ml H_2O). For the PVA solution to completely dissolve and produce a clear solution, it was stirred on a magnetic stirrer for several hours. Then, the prepared Fe_3O_4@SiO_2 NPs were added with different concentrations, 2, 4, and 6 wt.% to the solution, and with the help of high strength ultrasonic probe, the NPs were distributed in the PVA solution. After that, the composite solutions were placed into Petri dishes and allowed to dry at 25 °C in a dry environment. The obtained PVA-Fe_3O_4@SiO_2 films have a thickness of about ~ 100 µm (measured via digital micrometer).

2.2 characterization

The diffraction pattern of the PVA film with different concentrations of Fe_3O_4@SiO_2 NPs was recorded via XRD model-BrukerD8 with $\lambda = 1.5418$ Å (Cu-Kα). The chemical bonds were identified by Fourier transform-infrared spectrometer (FTIR, 4000–400 cm^{-1}), model-Vertex70-Bruker. Using an OLYMPUS-BX51 optical microscope, the morphology of the Fe_3O_4@SiO_2 in the PVA matrix was demonstrated. Using a Cary 5000-UV spectrophotometer, the UV–visible spectra were obtained.

3 Results and discussions

3.1 XRD analysis

Figure 1 depicts the XRD patterns of PVA films doped with various contents of Fe_3O_4@SiO_2 NPs.

After Fe_3O_4@SiO_2 additive to the PVA, the broad hump at $2\theta \sim 19.62°$, which refers to the (101) plane of the PVA (Parthasarathy et al. 2021), descends and broadens. This indicates that the Fe_3O_4@SiO_2 additions have decline the PVA's semi-crystallinity. The semi-crystallinity of PVA is caused by its hydroxyl groups, which react with additives to form new bonds (Siva et al. 2022). The reduction of the characteristic peak of pure PVA after the inclusion of Fe_3O_4@SiO_2 is associated with the expansion of the C–C chain, as expressed elsewhere (Ali et al. 2021; Zhu et al. 2013). Moreover, a small intense beak appeared at 35.57° with additive 2% Fe_3O_4@SiO_2 NPs, which became more pronounced with increasing the Fe_3O_4@SiO_2 NPs concentration, and additional beaks appeared as shown in the pattern. The peaks at $2\theta = 30.19°$, 35.57°, 43.36°, 57.25° and 62.81° are related to the (220), (311), (400), (511) and (440) diffraction planes of Fe_3O_4—cubic structure (reference card# JCPDS: 01–82–1533 (Divya et al. 2022)).

Additional investigation to the (101) diffraction plan was performed to investigate Fe_3O_4@SiO_2 NPs' impact on the XRD parameters of the PVA. The gaussian fitting (Fig. 2) helpful tool to investigate the fullwidth at half maximum of (101) diffraction plan ($FWHM_{(101)}$) and the diffraction angle of (101) diffraction plan ($\theta_{(101)}$). The crystallite size, $D_{(101)}$, dislocation

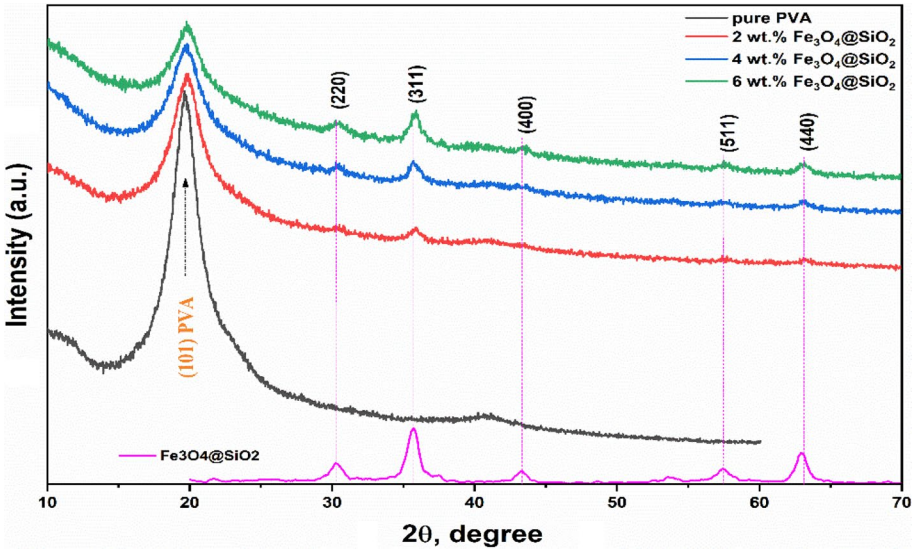

Fig. 1 XRD pattern of PVA-Fe_3O_4@SiO_2 nanocomposite films

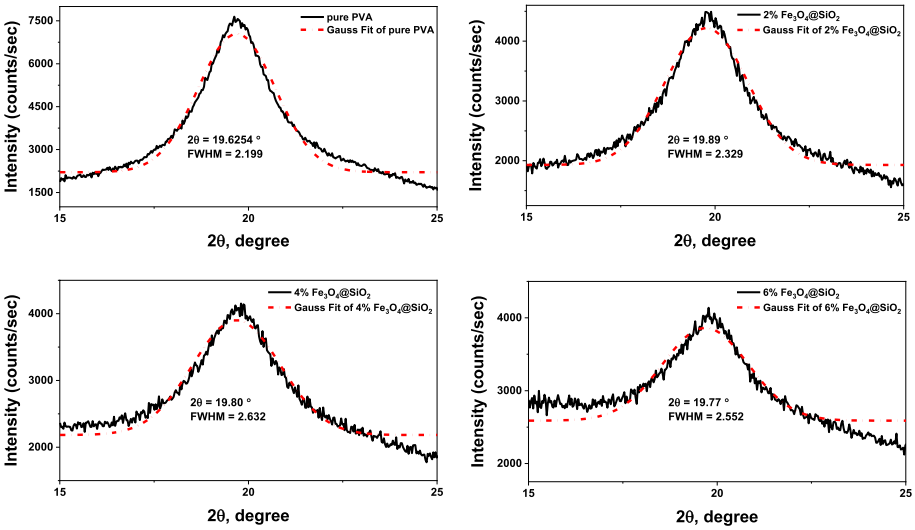

Fig. 2 Gauss fit of (101) peak of pure PVA and PVA-Fe_3O_4@SiO_2 films

density, δ, and the internal strain, ε, are calculated through the following equations (Ismail et al. 2022),

$$D_{(101)} = \frac{0.9\lambda}{FWHM_{(101)}cos\theta_{(101)}} \quad (1)$$

$$\delta = \frac{1}{D^2_{(101)}} \tag{2}$$

$$\varepsilon = \frac{FWHM_{(101)}}{4\tan\theta_{(101)}} \tag{3}$$

The obtained data are presented in Table 1.

The $D_{(101)}$ value decreases as the Fe_3O_4@SiO_2 NPs content increases in the PVA. The additives of Fe_3O_4@SiO_2 NP to the PVA matrix enlarge the C–C chain, the polymer layers are far apart, and the degree of crystallinity decreases consequently (Ali et al. 2021; Ali and Khairy 2019). Such result is in match with the literature (Ali et al. 2021; Zhu et al. 2013; Ali and Khairy 2019; Ali 2019; Shaalan et al. 2021; Badawi et al. 2022). Furthermore, agglomerations of Fe_2O_3@SiO_2 NPs and increases in their diameters cause additional peaks to appear at higher concentrations. Also, the other optical parameters, like ε and δ, were increased as the Fe_3O_4@SiO_2 concentration increased in the PVA matrix.

To confirm the decrease of the crystallinity index (CI) of the PVA matrix with the addition of Fe_3O_4@SiO_2, the area under the crystalline peaks (A_c) and the area under both crystalline and amorphous peaks (A_s) were used throughout the following equation (Sayed and Saber 2022);

$$CI, \% = \frac{A_c}{A_s} \times 100\% \tag{4}$$

The crystallinity index was calculated and summarized in Table 1. As shown, *CI* was decreased with the additives of Fe_3O_4@SiO_2 to the PVA matrix. From all the calculations and investigated parameters, one can conclude that adding Fe_3O_4@SiO_2 leads to a decrease in the PVA crystallinity.

3.2 FT-IR analysis

Figure 3 displays the FT-IR spectra of Fe_3O_4@SiO_2 and PVA-Fe_3O_4@SiO_2 films. Fe_3O_4@SiO_2 spectrum shows the characteristic peak at 1626 cm^{-1} assigned to the combination of the silanol group on the SiO_2 surface with the H–O–H bond of Fe_3O_4 NPs. It testifies to H-bond formation between the Fe_3O_4 and SiO_2 (Khalid et al. 2023). The broadband at 1408 cm^{-1} is attributed to the bond between -Fe and -COO, and the main peaks at 543 and 435 cm^{-1} are assigned to the Fe–O bond (Jannah et al. 2017). The pure PVA spectrum shows a broad peak at 3272 cm^{-1} for stretching vibration of O–H moieties due to the intra- and

Table 1 XRD geometrical parameters

Sample ID	$D_{(101)}$, nm	ε	δ, nm^{-2}	d-spacing, nm	Crystallinity index, %
pure PVA	3.83	0.055	0.068	0.4519	56
2%	3.62	0.058	0.076	0.4459	46
4%	3.19	0.066	0.098	0.4479	44
6%	3.30	0.064	0.092	0.4486	40

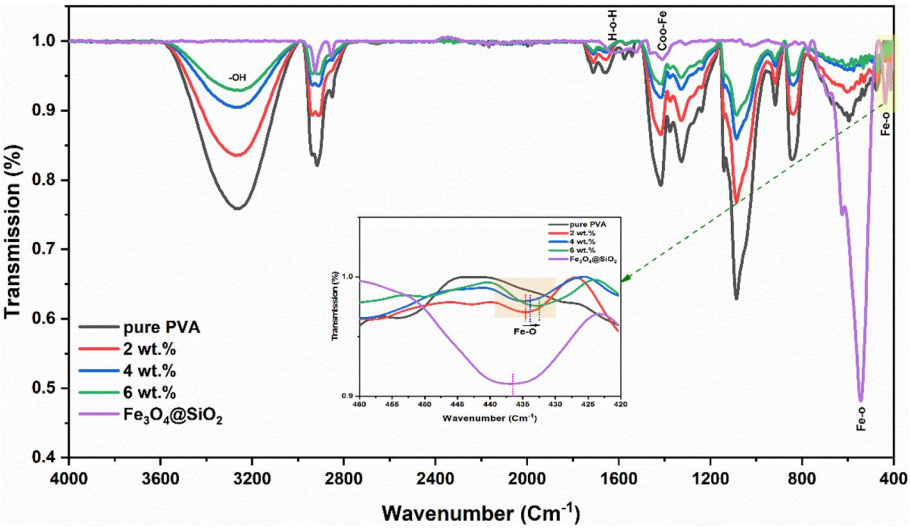

Fig. 3 FT-IR spectra of Fe_3O_4@SiO_2 NPs and PVA-Fe_3O_4@SiO_2 films

extra-molecular hydrogen bonding. Bands at 2917, 1717, 1660, 1414, and 845 cm^{-1} are called C–H (CH_2 asymmetric stretching), C=O stretching, C=C stretching, C–H bending, and C–C stretching, respectively. The intensity of all bands decreases as the Fe_3O_4@SiO_2 concentration increases in the PVA matrix. In addition, the band at 436 cm^{-1} related to the Fe–O band appeared in the PVA spectrum with the Fe_3O_4@SiO_2 additives to the PVA matrix (inset of Fig. 3). This band was slightly shifted to a lower wavenumber at 434, 433, and 432 cm^{-1} for 2, 4, and 6 wt.% Fe_3O_4@SiO_2, respectively. This is caused due to the complexation and cross-linking between Fe_3O_4@SiO_2 NPs and PVA molecules (Aziz et al. 2019; Ali 2019).

3.3 Optical microscope

Figure 4 shows the bright-field optical microscope images for PVA-Fe_3O_4@SiO_2 films. Figure 4a shows the PVA film without imperfections before adding Fe_3O_4@SiO_2 NPs. And Fig. 4b–d show PVA films doped with various Fe_3O_4@SiO_2 concentrations. The Fe_3O_4@SiO_2 NPs agglomerates and forms clusters when doped in the PVA matrix. The size and number of these clusters increase as the Fe_3O_4@SiO_2 concentration in the PVA rises. This could be due to the magnetic induction between the nanoparticles. Figure 4e shows the cluster size distribution in the polymer matrix, which shows a growth of the particle size of approximately 36, 40, and 64 µm for 2, 4, and 6 wt.% Fe_3O_4@SiO_2 NPs, the maximum size in the bright field images.

3.4 Optical properties

3.4.1 Absorption, interband transitions, and skin depth

The computed optical bandgap, index of refraction, and dispersion parameters are critical instruments for fabricating innovative materials, particularly for developing optical

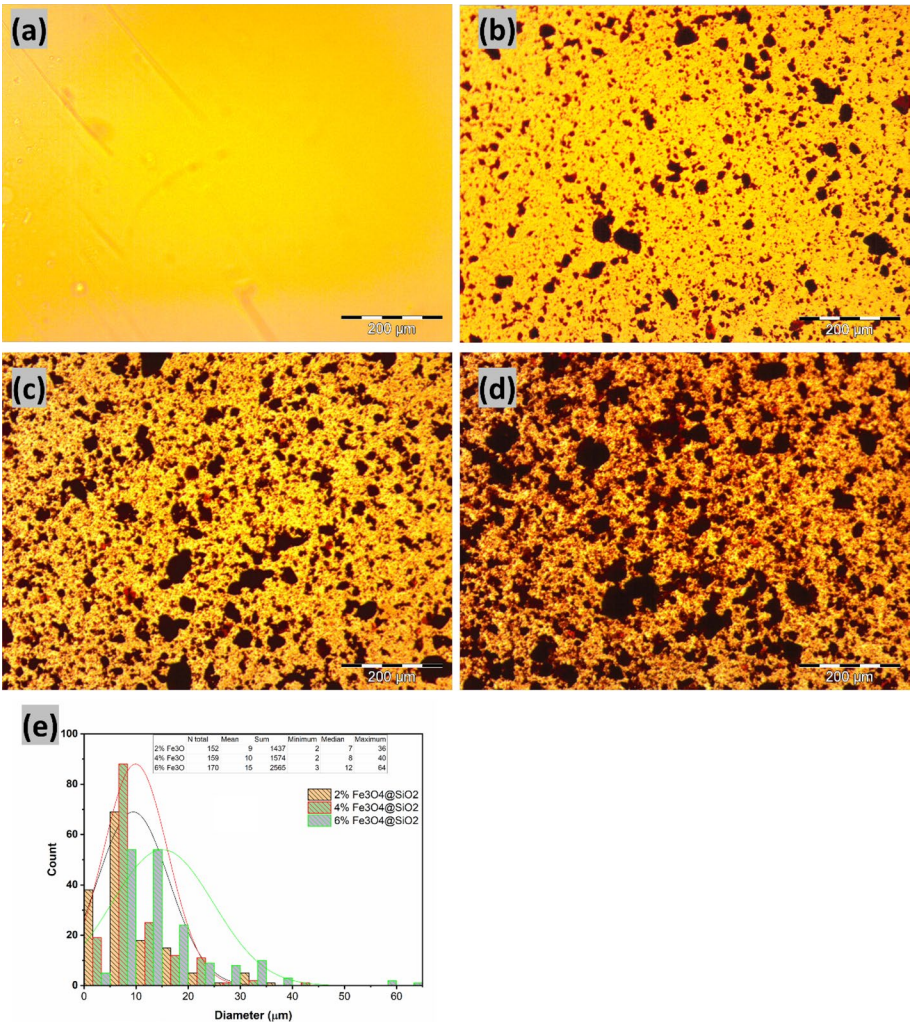

Fig. 4 Optical microscope images of all samples with 10 × magnification of PVA-Fe_3O_4@SiO_2; **a** 0, **b** 2, **c** 4, **d** 6 wt.% Fe_3O_4@SiO_2 NPs, and **e** the histogram curves

devices. These parameters are based on electronic absorption transitions investigated through the UV–visible spectrophotometer. Figure 5a illustrates the absorption variation with the wavelength (λ) for various Fe_3O_4@SiO_2 NPs concentrations doped in PVA. The $\pi \rightarrow \pi^*$electron transition can explain the characteristic absorption band of PVA observed at 274 nm, as depicted in the inset in Fig. 5a. This behavior aligns well with the literature (El-Khodary 2009). Also, the absorption spectrum of pure PVA has a distinct absorption edge, which points to the semi-crystalline nature of the PVA film, as confirmed previously from the XRD results. This is evidenced by the fact that the absorption edge is sharp (Choudhary and Sengwa 2019). Increasing Fe_3O_4@SiO_2 content in the host matrix caused an enhancement of its absorption. This result can be ascribed to electronic transitions between the NPs and the polymeric host matrix (Moumen et al. 2019). In other words, this result can be due to the scattering by NPs doped

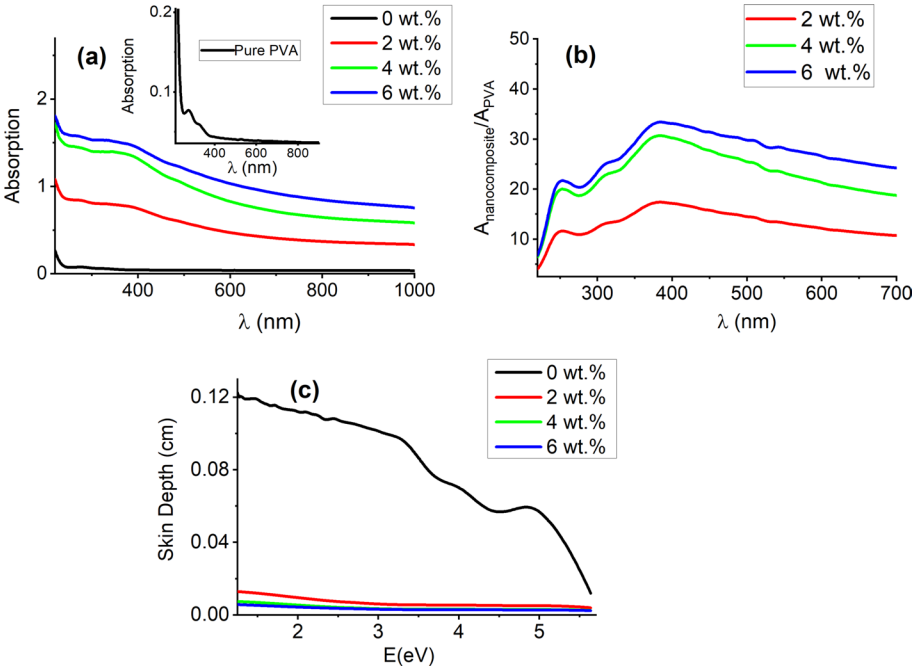

Fig. 5 Variation of **a** absorption and **b** $A_{nanocomposite}/A_{PVA}$ on (λ) for different Fe_3O_4@SiO_2 content in PVA. **c** δ vs. energy (E) for different Fe_3O_4@SiO_2 NPs content in PVA. The inset represents the variation of the absorption spectra

in PVA, which have a particle size smaller than the incident wavelength (Fasasi et al. 2018).

Absorption peaks of Fe_3O_4@SiO_2 NPs were not readily apparent in the absorption spectra (Fig. 5a) but were visualized by plotting the absorption of PVA-Fe_3O_4@SiO_2 divided by the PVA absorption versus (λ) (Fig. 5b). Figure 5b illustrates two broad absorption peaks at (250 nm &380 nm), (253 nm & 383 nm), and (255 nm & 389 nm) corresponding to 2, 4, and 6 wt. % of Fe_3O_4@SiO_2 NPs doped in PVA, respectively. These findings are consistent with the authors' previously published work (Khalid et al. 2023), which showed absorption peaks of un-doped Fe_3O_4@SiO_2 NPs at 234 and 387 nm.

The skin depth (δ) is the distance an electromagnetic wave penetrates a substance, which can be computed as follows: $\delta = \frac{1}{\alpha}$, as α is the absorption coefficient ($\alpha = \frac{2.303 \times Absorbance}{samplethickness}$) (Ahmed et al. 2020a). Figure 5c shows the variation of δ with the incident energy for different Fe_3O_4@SiO_2 concentrations doped in PVA. The δ values recorded at constant energy (1.3 eV) and displayed in Table 2, for 0, 2, 4, and 6 wt.% Fe_3O_4@SiO_2 doped in PVA are 0.120, 0.013, 0.007, and 0.006 cm, respectively. The decreased δ of nanocomposites can be explained by increasing Fe_3O_4@SiO_2 content in the PVA, which increases the absorption and decreases the transparency.

Tauc bandgap energy (E_{gab}^{Tauc}), incident photon energy (E), and optical absorption coefficient (α) are related in Tauc's equation for α greater than 10^4 cm^{-1}, according to the following relation (Badawi et al. 2017; Ahmed 2010):

Table 2 The values of optical parameters (E_{gap}^{Tauc}), (E_{gap}^{ASF}), (E_u), (S), ($E_{e\text{-}ph}$), and (N)

Optical parameter	Current work				Previously published works					
	Content of Fe_3O_4@SiO_2 (wt.%) doped in PVA				TiO_2/PVA (eV) (Mohammed et al. 2019)	ZnO/PVA (eV) (Mohammed et al. 2019)	2 wt.% of iron oxide /PVA Donya et al. (2020)	1wt.% of Fe_2O_3-rGO /PVA Ahmed et al. (2023)	6 wt.% of SiO_2 / PVA Soliman et al. (2020)	Fe_3O_4@ SiO_2 Khalid et al. (2023)
	0	2	4	6						
δ cm (at 1.3 eV)	0.120	0.013	0.007	0.006						
E_{gap}^{ASF}(eV)	5.38	4.91	4.85	4.54						5.95
E_{gap}^{Tauc}(eV)	5.39	5.05	4.88	4.52	5.20	4.80	3.74	4.29	5.40	5.97
E_u(eV)	0.39	1.78	2.05	3.21				0.76	0.59	1.70, 0.53
$Sx10^{-2}$	6.69	1.46	1.27	0.81				3.43		
$E_{e\text{-}ph}$	9.96	45.4	52.3	82.0				19.42		
$N=(34.3/E_{direct}^{Tauc})^2$	40	46	49	58				64		

$$\alpha E = B(E - E_{gab}^{Tauc})^{K} \quad (5)$$

where B is constant, and K donates the electronic transition nature. Based on the kind of electronic transition, K can have the values 2 and ½, respectively, for indirect and direct allowed transitions. Figure 6a represents $(aE)^2$ versus the incident photon-energy for different Fe_3O_4@SiO_2 NPs content in PVA. A linear behavior was obtained from the plot in Fig. 6a**,** evidence of the direct allowed transition. The E_{gab}^{Tauc} was estimated based on the linear fit intercept with the x-axis (see Fig. 6a). The obtained E_{gab}^{Tauc} were listed in Table 2.

Under the absorption spectra, the optical band gap was successfully estimated using the absorption spectrum fitting (ASF) approach (Khalil et al. 2023):

$$\alpha(\lambda) = B(hc)^{-1+K}\lambda\left(\lambda^{-1} - \lambda_g^{-1}\right)^{K} \quad (6)$$

where h, c, and λ_g are Plank's constant, the speed of light, and the wavelength at which the optical gap appears, respectively. The best match at K equals one-half, indicating that all samples undergo direct allowed transition. Extrapolating the linear section of $(A\lambda^{-1})^{1/K}$ plot versus λ^{-1}, at $(A\lambda^{-1})^{1/K}=0$, yielded the value of λ_g^{-1}, shown in Fig. 6b. Table 2 displays the E_{gap}^{ASF} values for all samples by multiplying 1239.83 byλ_g^{-1}. The values of E_{gap}^{ASF} are 5.38, 4.91, 4.85, and 4.54 eV, respectively, for 0, 2, 4, and 6 wt.% of Fe_3O_4@SiO_2 doped in PVA. Also, the values of E_{gap}^{Tauc} decreased from 5.39 eV for the pure PVA to 4.52 eV for 6wt.%Fe_3O_4@SiO_2-PVA. The decrease of the bandgap is well consistent with earlier research's findings of PVA/CuO (Selvi et al. 2019), PVA/Al_2O_3 (Sugumaran et al. 2015), and PVA/iron oxide (Donya et al. 2020). The obtained findings from both E_{gab}^{Tauc} and E_{gab}^{ASF}

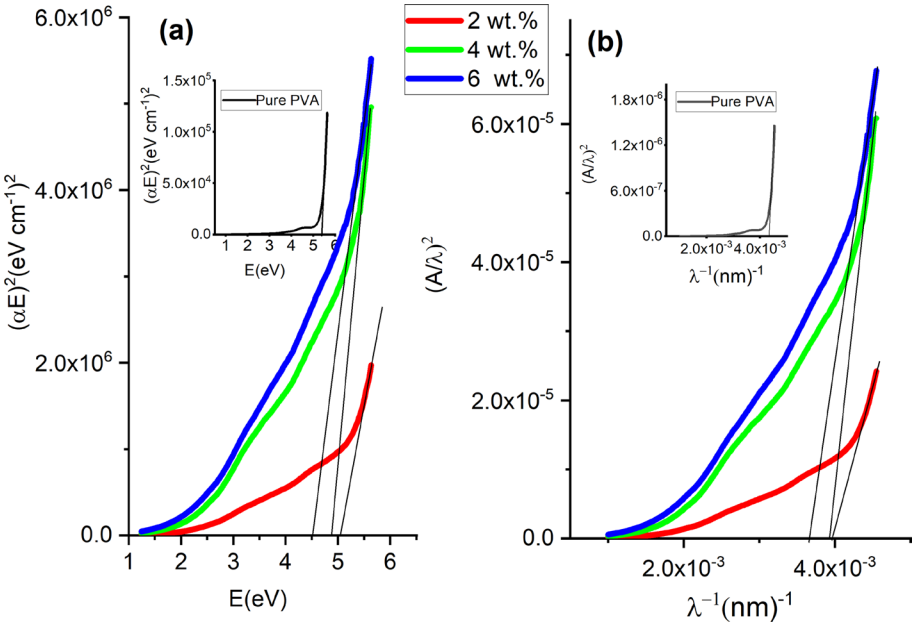

Fig. 6 **a** $(\alpha E)^2$ vs. energy (E). **b** Plotting $(A/\lambda)^2$ versus $(1/\lambda)$ for different Fe_3O_4@SiO_2 NPs content in PVA. The insets are for pure PVA

are close to each other. Reducing the energy gaps of PVA by increasing the Fe_3O_4@SiO_2 additives can be attributed to more defects formation in the nanocomposites due to the formation of unsaturated bonds (Aslam et al. 2017). Creating localized states within the bandgap and changes in the disordering degree in the PVA may also be responsible for the bandgap's reduction (Choudhary 2018). As trapping and recombination centers, the localized states within the bandgap alter its structure (Abdullah et al. 2015). Table 2 compares some optical properties derived in the current work with those found in the literature.

Urbach energy (E_u) analysis confirms the degree of disorder change. It can be described by the relationship given below (Abdelrazek et al. 2018):

$$\alpha = \alpha_o \exp\left(\frac{E}{E_u}\right) \tag{7}$$

where α_o and E_u are, respectively, a constant and Urbach energy. The variation of ln(α) versus the photon energy (E) for pure PVA (an example for other samples) is illustrated in Fig. 7a. The E_u value was estimated from the inverse of the slope of the straight lines. Increasing Fe_3O_4@SiO_2 content in PVA leads to higher E_u values, as seen in Table 2. The existence of defects and a narrowing of the bandgap are indicated by a growing Urbach tail or Urbach energy due to doping. This outcome agrees quite well with previous research (Goumri et al. 2016; Rathod et al. 2016; Ahmed 2017, 2014).

Figure 7b, c shows the dependence of E_u on the bandgap deduced by Tauc and ASF methods. Linear equations intercept given from the linear fitting between E_u and E_{gap}^{Tauc}, and E_{gap}^{ASF} are 17.6 ± 1.4 eV, and 18.2 ± 0.93 eV, respectively. In the absence of E_u, these intercept values represent the typical energy gap.

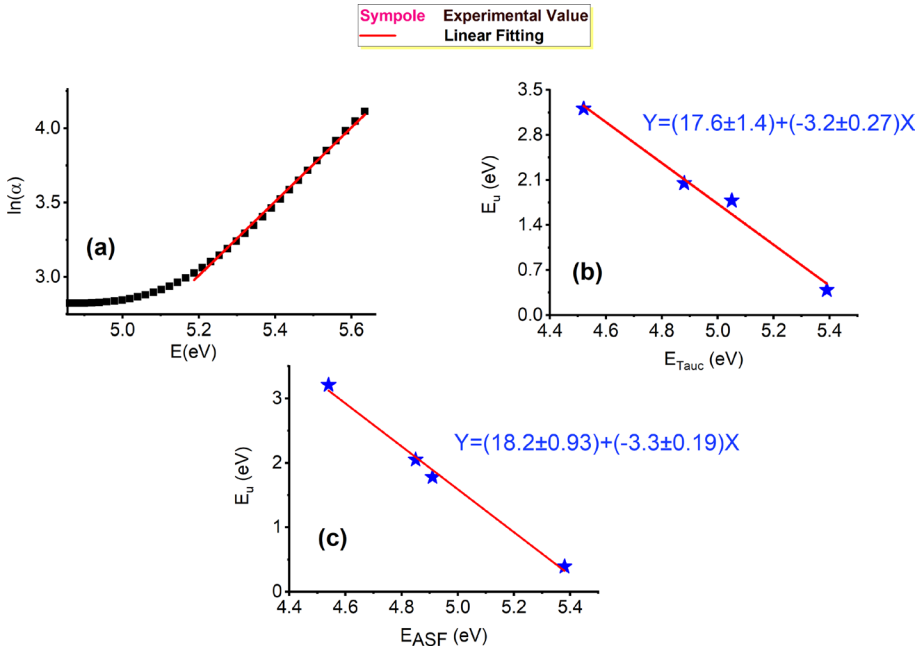

Fig. 7 **a** ln(α) vs. (E) for pure PVA. E_u variation with **b** E_{Tauc} and **c** E_{ASF} for variant Fe_3O_4@SiO_2 contents in PVA

The electron–phonon strength (Ee-ph) interactions determine the absorbance edge broadening. It can be calculated using the steepness parameter (S) from the following equations (Raja et al. 2003; Skettrup 1978):

$$S = \frac{T_{room}K_B}{E_{Tail}};\ E_{e-ph} = \frac{2}{3}S^{-1} \tag{8}$$

where T_{room} is the room temperature, and k_B is the Boltzmann constant. The S and $E_{e\text{-}ph}$ values are tabulated in Table 2. The S value decreases by increasing the Fe_3O_4@SiO_2 concentrations in PVA, and the highest value was detected in pure PVA (0.067). Nevertheless, the values of $E_{e\text{-}ph}$ of the nanocomposites increased from 9.96 for pure PVA to 82.0 for the highest content of the NPs doped in the polymeric host matrix. Consequently, increasing the doping of NPs in PVA caused an increase in the filled bands (Al-Bataineh et al. 2020).

Several attempts have been made to find a universal technique for correlating the refractive index (n) and optical band gap (E_g) to help understand the band structure of the studied nanocomposites. Ravindra, et al. ($n_{R,etal}$), Moss (n_M), Kumar- Singh ($n_{K,S}$), Anani, et al. ($n_{A,etal}$), Hervé -Vandamme ($n_{H,V}$), Tripathy (n_T), Reddy-Ahammed ($n_{R,Ah}$), (Tripathy 2015; Kumar and Singh 2010; Hervé and Vandamme 1994; Anani et al. 2008; Reddy and Nazeer Ahammed 1995; Ravindra et al. 1979; Moss 1985) are some different models used in this study to correlate between the refractive index (n) and optical band gap (E_g) as the following:

$$n^4_{Retal.} = 108 \times E_g^{-1} \tag{9}$$

$$n^4_M = 95 \times E_g^{-1} \tag{10}$$

$$n_{K,S} = 3.3668 \times E_g^{-0.32234} \tag{11}$$

$$n_{A,etal.} = 3.4 - 0.2E_g \tag{12}$$

$$n_{H,V} = \sqrt{1 + \left(\frac{13.6}{E_g + 3.4}\right)^2} \tag{13}$$

$$n_T = \left[1 + (1.9017 \times \exp(-0.539 \times E_g))\right] \times 1.73 \tag{14}$$

$$n^4_{R,Ah} = 154(-0.365 + E_g)^{-1} \tag{15}$$

$$n_{average} = [n_{R,etal} + n_M + n_{K,S} + n_{A,etal} + n_{H,V} + n_T + n_{R,Ah}] \div 7 \tag{16}$$

By using E^{Tauc}_{gap}, the theoretical linear refractive index (n) values, estimated from these models, are illustrated in Fig. 8 for different Fe_3O_4@SiO_2 concentrations doped in PVA. The average refractive index ($n_{average}$) has values of 2.07, 2.12, 2.15, and 2.20, corresponding to 0, 2, 4, and 6 wt.% of NPs doped in PVA, respectively. Moreover, the models' estimated values of n for the examined nanocomposites are identical, and adding NPs increases their influence.

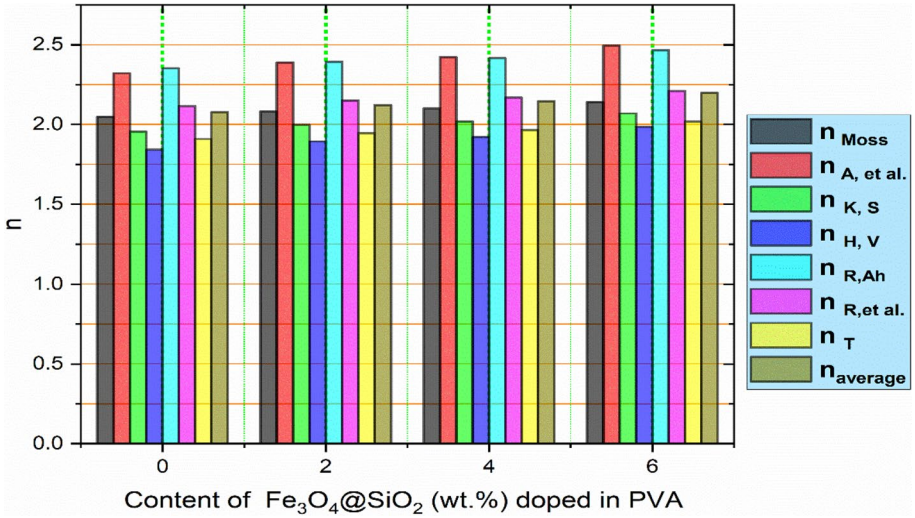

Fig. 8 Plotting the refractive index (n) versus Fe_3O_4@SiO_2 NPs content doped in PVA (regarding various theoretical models using $E_{(Tauc)}$)

3.4.2 Refractive index (n) and attenuation coefficient (k)

The index of refraction, n, is crucial for examining a material's optical qualities. The refractive index of polymeric materials is fascinating because of its relationship with the local electric field and electronic polarizability. It also determines the materials' compatibility with optoelectronic devices. Based on the reflection (R) and attenuation coefficient (k), the refractive index was computed as follows (Aziz et al. 2019; Ahmed 2009; Abdullah et al. 2016):

$$R = 1 - \sqrt{\text{transmission} \times \exp(absorption)} \tag{17}$$

$$k = \frac{\alpha\lambda}{4\pi} \tag{18}$$

$$n = \left(\frac{1+R}{1-R}\right) + \sqrt{\frac{4R}{(1-R)^2} - k^2} \tag{19}$$

Figure 9a shows the nanocomposites' attenuation coefficient (k) depending on wavelength. It is observed that as the Fe_3O_4@SiO_2 content in PVA increased, the k value increased. With an increase in incident wavelength, the k values increased due to the interaction between the polymeric material and the incident light. This behavior agrees with some published works (Jebur et al. 2020; Hashim 2020; Ahmed et al. 2020b).

The (n) dependence on (λ) for all samples is depicted in Fig. 9b. For 0, 2, 4, and 6 wt.% of Fe_3O_4@SiO_2 doped in the PVA, the n values are 1.8, 14.4, 40.7, and 62.9, respectively, detected at 500 nm. An enhancement in the refractive index of the nanocomposites of Fe_3O_4@SiO_2/PVA was investigated in this study compared to some previous publications, including GO/PVA nanocomposites (Aslam et al. 2017), $AgAlO_2$/PVA nanocomposites

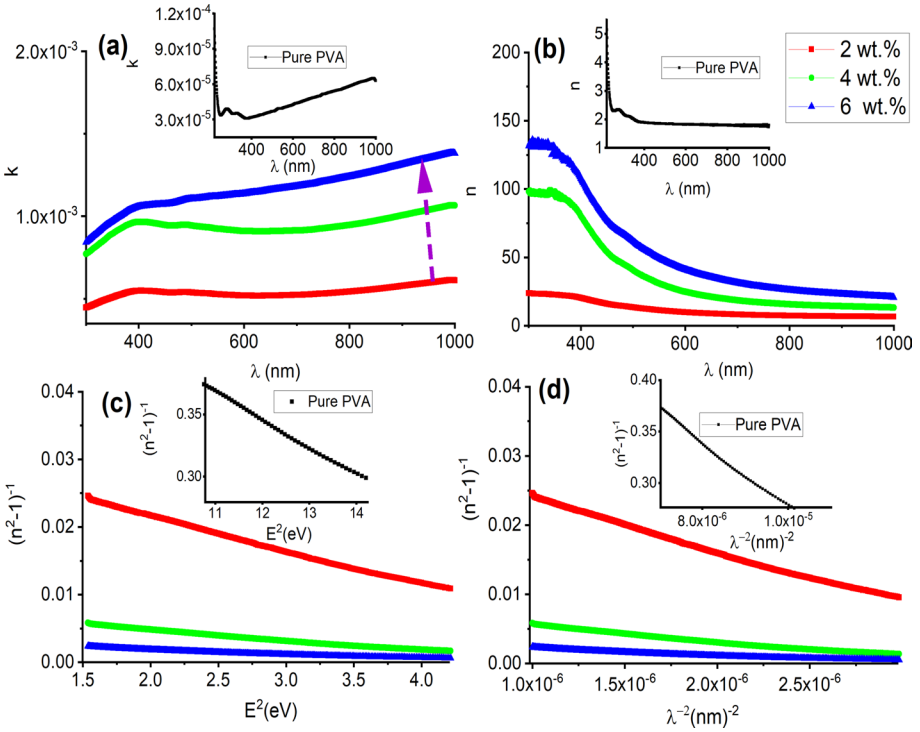

Fig. 9 Plots of; **a** attenuation coefficient (k) and **b** refractive index (n) on the incident wavelength. The variation of **c** $(n^2\text{-}1)^{-1}$ vs. E^2, and **d** $(n^2\text{-}1)^{-1}$ vs. λ^{-2}, for the different Fe_3O_4@SiO_2 NPs content doped in PVA

(Somesh et al. 2019), CeO_2/PVA nanocomposites (Aziz et al. 2021), and Fe_2O_3@reduced graphene oxide/PVA nanocomposites (Ahmed et al. 2023). The n value increases as Fe_3O_4@SiO_2 concentrations increase in PVA due to the formation of intermolecular bonds between PVA and Fe_3O_4@SiO_2 NPs (Sayed et al. 2014).

3.4.3 Optical dispersion parameters

Wemple-DiDomenico's single effective oscillator model was able to investigate refractive index dispersion by applying the following formula (Abdulwahid et al. 2016; Wemple and DiDomenico 1971):

$$n^2(E) = 1 + \frac{E_d E_o}{E_o^2 - E^2} \tag{20}$$

where E_o is the single oscillator energy, and E_d is the dispersion energy, which defines the strength of optical transitions in the inner band. The values of E_d and E_o were calculated by graphing $(n^2\text{-}1)^{-1}$ vs. E^2 for each of the nanocomposites that were scrutinized, as demonstrated in Fig. 9c. The Fe_3O_4@SiO_2 additive to PVA yields a decrease in E_o values and an increase in E_d values. The PVA-6 wt.%Fe_3O_4@SiO_2 film displayed the highest value of E_d (579 eV) and the lowest value of E_o (2.03 eV). Furthermore, E_{gab}^{Tauc} equals almost E_o of PVA. However, in the case of all nanocomposites of Fe_3O_4@SiO_2 NPs (2, 4, 6 wt.%)/

PVA, the values of E_{gab}^{Tauc} equals nearly twice the values of E_o. Additionally, the formula for the static refractive index ($n_o = n$ at $E = 0$ in Eq. (20)) was derived as follows (Habubi et al. 2013):

$$n_o = \sqrt{1 + \frac{E_d}{E_o}} \tag{21}$$

The listed values of n_o in Table 3 show that the highest value was detected to pure PVA (1.64), and the lowest value was determined to be 6wt.% of Fe_3O_4@SiO_2 NPs (16.9). Moreover, optical oscillator strength, *f,* describes the efficiency with which the initial and final states of electrons absorb photon energy according to the following equation (Güneri and Kariper 2012):

$$f = E_o E_d \tag{22}$$

The *f* highest value was observed for PVA-6 wt.% Fe_3O_4@SiO_2 film (1175 eV^2), as observed in Table 3**.**

Understanding optical spectrum moments M_{-1} and M_{-3} helps explain inter-band transition strengths. Dielectric constants and effective valence electrons are connected to these characteristics. The optical spectrum moments can be calculated using the following relations (Mahdi and Al-Ani 2012):

$$E_o^2 = \frac{M_{-1}}{M_{-3}} \tag{23}$$

$$E_d^2 = \frac{M_{-1}^3}{M_{-3}} \tag{24}$$

Table 3 shows that the values of M_{-1} and M_{-3} increased by increasing the content of the Fe_3O_4@SiO_2 NPs. The M_{-1} and M_{-3} highest values were observed for 6wt.% of Fe_3O_4@SiO_2 NPs/PVA nanocomposite, which are 285 and 69.21, respectively. However, the infinite wavelength refractive index (n_∞), the average inter-band oscillator wavelength (λ_o), and oscillator strength (S_o) were computed using the Moss model. The three parameters of the Moss model were computed from the following relations (Ahmed et al. 2020b):

$$\frac{(n_\infty^2 - 1)}{(n^2 - 1)} = 1 - \frac{\lambda_o^2}{\lambda^2} \tag{25}$$

Table 3 The Wemple-Didomenico oscillating parameters, including the values of E_o, E_d, n_o, *f*, (M_{-1} and M_{-3}), (S_o), (λ_o), and (n_∞), for PVA-Fe_3O_4@SiO_2 nanocomposites

Sample (wt.%)	E_d (eV)	E_o (eV)	n_o	f $(eV)^2$	M_{-1}	M_{-3}	$S_o \times 10^{-5}$ $(nm)^{-2}$	λ_o (nm)	n_∞
0	9.22	5.42	1.64	49.97	1.70	0.058	3.10	232	1.6
2	79.1	2.53	5.68	200.1	31.3	4.884	13.2	487	5.7
4	279	2.24	11.2	624.9	125	24.82	38.5	570	11
6	579	2.03	16.9	1175	285	69.21	82.6	597	17

$$n_{\infty}^{2} = 1 + S_o \lambda_o^2 \tag{26}$$

Equation (25) was rewritten as follows:

$$\left(n^2 - 1\right) = \frac{S_0 \lambda_0}{1 - \left(\frac{\lambda_0}{\lambda}\right)^2} \tag{27}$$

For all samples being examined, the variation of $(n^2 - 1)^{-1}$ with $1/\lambda^2$ is illustrated in Fig. 9d. The intercept of the plot in Fig. 9d provided the $(S_o \lambda_o^2)^{-1}$ value. However, the slope gives the $(1/S_o)$ value. As shown in Table 3, the S_o, λ_o, and n_∞ are Fe_3O_4@SiO_2 dependent. The nanocomposite of 6 wt.% of Fe_3O_4@SiO_2/PVA has the highest values of S_o, λ_o, and $n_{\infty,}$ which are 82.6×10^{-5} nm^{-2}, 597 nm, and 17, respectively.

3.4.4 Optical dielectric parameters

The complex function of dielectric (ε*) is a sum of real (ε_r) and imaginary (ε_i) components. These two parameters depended on (n) and (k) according to the following relations (Suma et al. 2017):

$$\varepsilon_r = n^2 - k^2; \varepsilon_i = 2nk \tag{28}$$

The (ε_i) characterizes the degree of light dissipation that occurs when it is transmitted through a substance. The value of (ε_r) is contingent upon the mobility of electrons during light transformation within the given medium (Abdullah et al. 2015). The dependence of (ε_r) and (ε_i) of complex dielectric function on (λ) for all samples are illustrated in Fig. 10a, b, respectively. The augmentation of Fe_3O_4@SiO_2 additives in PVA causes an enhancement in ε_r and ε_i values. The change in the ε_i values can be explained by the alternation in the polymeric substance's dipole motion (Suma et al. 2017). Adding Fe_3O_4@SiO_2 NPs to PVA causes a shift in the ε_r values. It can be attributed to the interactions between the incident photon and the free electron in the nanocomposites (Wise 1998). At wavelengths greater than 700 nm, the values of ε_r exhibit a lack of wavelength dependence. This behavior can be attributed to the molecules in the samples' inability to track the incident field fluctuations (Sayed et al. 2014) effectively. On the other hand, at wavelengths lower than 700 nm, the wavelength dependency of ε_r and ε_i is related to the interactions between the incident photons and free-electrons (Shehap and Akil 2016).

3.4.5 Surface and volume energy loss functions

The energy dissipation was characterized using two parameters: (i) the surface energy loss function (SELF) and (ii) the volume energy loss function (VELF). The term SELF describes the likelihood that as fast electrons traverse a surface, they will experience energy loss. However, the absence of rapid electron energy during a material's transmission can be understood from the VELF. The SELF and VELF values were calculated from the following equations (Abdel-Salam et al. 2022; Sarkar et al. 2014):

$$VELF = \frac{\varepsilon_i}{\varepsilon_r^2 + \varepsilon_i^2}; SELF = \frac{\varepsilon_i}{(\varepsilon_r + 1)^2 + \varepsilon_i^2} \tag{29}$$

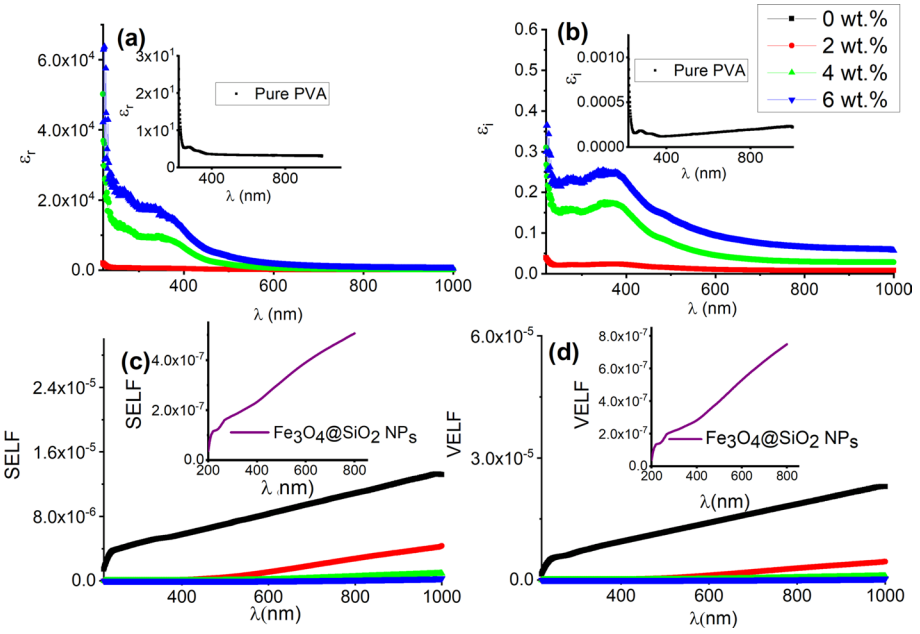

Fig. 10 For the different nanocomposites of PVA-Fe_3O_4@SiO_2, the dependence of **a** (ε_r), and **b** (ε_i), **c** SELF, and **d** VELF on the incident wavelength. The insets are the **c** SELF and **d** VELF of Fe_3O_4@SiO_2 NPs

The SELF and VELF dependences on (λ) for all samples under investigation are shown in Fig. 10c, d, respectively. The insets in Fig. 10c, d are the SELF and VELF of Fe_3O_4@SiO_2 NPs. At a constant wavelength of 800 nm, the values of VELF are 1.86×10^{-5}, 2.87×10^{-6}, 5.01×10^{-7}, and 1.43×10^{-7}, whereas the values of SELF are 1.08×10^{-5}, 2.76×10^{-6}, 4.96×10^{-7}, and 1.41×10^{-7} for 0 wt.%, 2 wt.%, 4 wt%, 6 wt.% of Fe_3O_4@SiO_2 NPs doped in PVA, respectively. The values of VELF and SELF of Fe_3O_4@SiO_2 NPs are 7.49×10^{-7} and 5.07×10^{-7}, respectively. The values of VELF and SELF of Fe_3O_4@SiO_2 NPs are lower than the corresponding values of PVA. Therefore, increasing the concentration of the doped nanoparticles resulted in reducing the values of VELF and SELF of the fabricated composites. The higher values of VELF than those of SELF resulted in fast electrons losing more energy during their movement inside materials than on their surfaces.

3.4.6 Linear and nonlinear optical parameters

The importance of nonlinear optical materials to the future of optical information processing technologies has garnered much interest. The nonlinearity of the materials is an intriguing and promising quality because it increases the variety of non-linear devices that can benefit from them (Sajid et al. 2023). The linear static refractive index (n_o) was calculated using E_{direct}^{Tauc} values according to the following relation (Dimitrov and Sakka 1996):

$$n_o = \left(\frac{(2C+1)}{(1-C)}\right)^{0.5}; C = -\left[\left(\frac{E_{direct}^{Tauc}}{20}\right)^{0.5}\right] + 1 \quad (30)$$

Figure 11a shows the dependence of (n_o) on the Fe_3O_4@SiO_2 content in PVA. The highest value was detected to 6 wt.%Fe_3O_4@SiO_2/PVA (2.07), and the lowest value was observed for pure PVA (1.94). For the relationship between n_o and Fe_3O_4@SiO_2 NPs content (wt. %), the following linear equation with $R^2=0.98$ is the best fit:

$$n_o = (1.94 \pm 0.007) + (0.02 \pm 0.002)X \tag{31}$$

where X is the Fe_3O_4@SiO_2 content in PVA.

Moreover, the high-frequency dielectric constant (ε_∞), for all samples under examination was determined by plugging the measured values of n_o into the following formula (Das et al. 2022):

$$\varepsilon_\infty = n_o^2 \tag{32}$$

The nanocomposite of 6 wt.% Fe_3O_4@SiO_2-PVA has the greatest value of ε_∞ (4.31) compared to the others, as observed in Fig. 11b. A linear equation is utilized to represent the optimal fitting for the correlation between ε_∞ and Fe_3O_4@SiO_2 NPs content, which is as follows:

$$\varepsilon_\infty = (3.8 \pm 0.03) + (0.08 \pm 0.008)X \tag{33}$$

where R^2 equals 0.98.

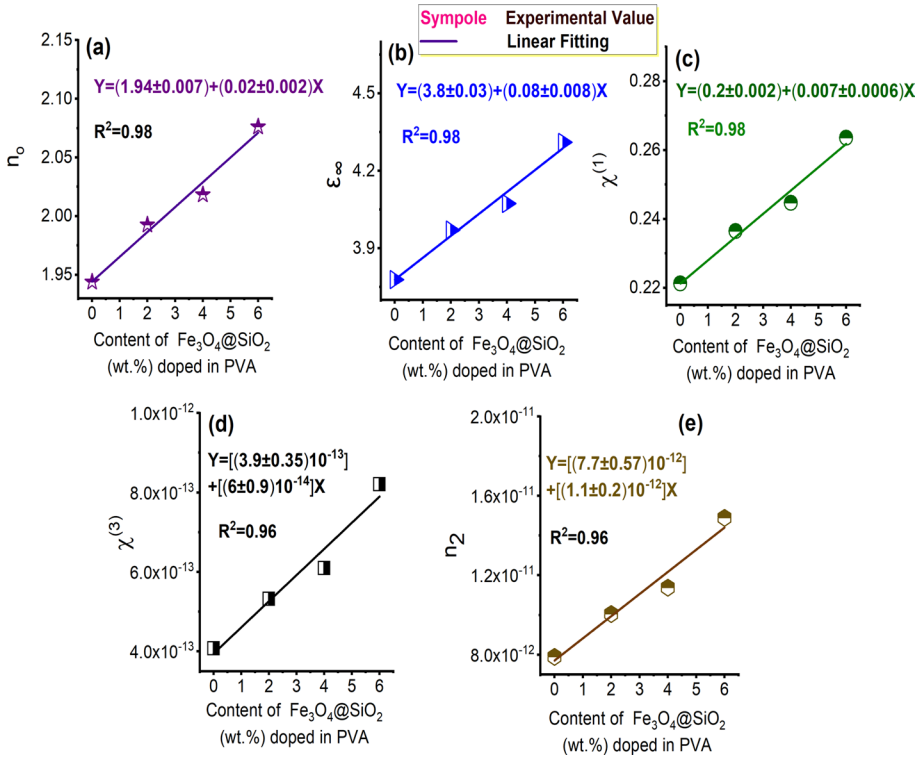

Fig. 11 **a** n_o, **b** ε_∞, **c** $\chi^{(1)}$, **d** $\chi^{(3)}$,and **e** n_2 vs. Fe_3O_4@SiO_2 content doped in PVA

The determination of the first ($\chi^{(1)}$) and third ($\chi^{(3)}$) ordered nonlinear susceptibility was conducted through the utilization of Miller's empirical rule (Yadav and Sharma 2015), which is outlined as follows:

$$\chi^{(1)} = \frac{(n_o^2 - 1)}{4\pi} \tag{34}$$

$$\chi^{(3)} = 1.7 \times 10^{-10} \left[\chi^{(1)}\right]^4 \tag{35}$$

Figure 11c illustrates that the highest value of $\chi^{(1)}$ was determined for 6 wt.% of Fe_3O_4@SiO_2 NPs/PVA nanocomposite (0.264). The correlation between $\chi^{(1)}$ and Fe_3O_4@SiO_2 NPs content is represented by a linear equation that provides the optimal fitting, expressed as follows:

$$\chi^{(1)} = (0.22 \pm 0.002) + (0.007 \pm 0.0006)X \tag{36}$$

Moreover, the $\chi^{(3)}$ value increases as the Fe_3O_4@SiO_2 concentrations increase, as displayed in Fig. 11d. The linear equation with an R^2 value of 0.96 is the most suitable fit for expressing the correlation between the content (wt. %) of Fe_3O_4@SiO_2 NPs and $\chi^{(3)}$:

$$\chi^{(3)} = \left[(3.95 \pm 0.35) \times 10^{-13}\right] + [(6.6 \pm 0.94) \times 10^{-14}]X \tag{37}$$

The following expression was used to determine the nonlinear refractive index (n_2) (Tichá and Tichý 2002):

$$n_2 = \frac{12\pi\chi^{(3)}}{n_o} \tag{38}$$

Figure 11e shows the dependence of (n_2) on the Fe_3O_4@SiO_2 content. The linear equation with an R^2 of 0.96 best describes the relationship between Fe_3O_4@SiO_2 NPs concentration (wt.%) and (n_2):

$$n_2 = \left[(7.7 \pm 0.57) \times 10^{-12}\right] + [(1.1 \pm 0.2) \times 10^{-12}]X \tag{39}$$

4 Conclusion

PVA-Fe_3O_4@SiO_2 films were fabricated via the casting method. The impact of Fe_3O_4@SiO_2 on the structure and optical parameters of the PVA film was investigated. The nature of PVA semi-crystallinity was found to decrease with an increase in Fe_3O_4@SiO_2 concentration and hydrogen bonding was created between PVA molecules and the surface of Fe_3O_4@SiO_2 as confirmed by RD and FT-IR techniques, respectively. The PVA absorption increases with increasing Fe_3O_4@SiO_2 concentration, affecting the polymer films' optical parameters. The bandgap decreased from 5.39 eV for PVA to 5.05, 4.88, and 4.52 eV for 2, 4, and 6 wt.% Fe_3O_4@SiO_2, respectively. The refractive index increased according to the rising material density with increasing Fe_3O_4@SiO_2 content into PVA. The PVA-Fe_3O_4@SiO_2 films are promising materials for various industrial applications. The nonlinear optical susceptibility and the nonlinear refractive index were calculated via the

Wemple-DiDominco model and were found to increase as the Fe_3O_4@SiO_2 concentration increased in the PVA matrix.

Author contributions TSS: conceptualization, formal analysis, investigation, methodology, data curation, writing—review & editing. AK: conceptualization, methodology, formal analysis, data curation, Writing—review & editing. MT: conceptualization, formal analysis, investigation, writing—original draft. RMA: conceptualization, formal analysis, investigation, methodology, data curation, writing—review & editing.

Funding There is no funding for this work.

Data availability All the data's available in the manuscript.

Declarations

Conflict of interest The authors declare that they have no competing financial interests or personal relationships that could have appeared to influence the work reported in this paper.

Ethical approval This article does not contain any studies with animals performed by any of the authors.

References

Abdelrazek, E.M.M., Abdelghany, A.M., Badr, S.I., Morsi, M.A.: Structural, optical, morphological and thermal properties of PEO/PVP blend containing different concentrations of biosynthesized Au nanoparticles. J. Mater. Res. Technol. **7**, 419–431 (2018). https://doi.org/10.1016/j.jmrt.2017.06.009

Abdel-Salam, A.I., Khalid, A., Awad, M.M., Hussein, Y., Ahmed, R.M.: Investigating the impact of growth time of CdSe quantum dots on the structure and optical properties of its nanocomposites with SiO_2 for improvement of optical devices. J. Alloys Compd. **925**, 166729 (2022). https://doi.org/10.1016/J.JALLCOM.2022.166729

Abdullah, O.G., Aziz, S.B., Omer, K.M., Salih, Y.M.: Reducing the optical band gap of polyvinyl alcohol (PVA) based nanocomposite. J. Mater. Sci. Mater. Electron. **26**, 5303–5309 (2015). https://doi.org/10.1007/S10854-015-3067-3/TABLES/3

Abdullah, O.G., Aziz, S.B., Rasheed, M.A.: Structural and optical characterization of PVA: $KMnO_4$ based solid polymer electrolyte. Results Phys. **6**, 1103–1108 (2016). https://doi.org/10.1016/J.RINP.2016.11.050

Abdulwahid, R.T., Abdullah, O.G., Aziz, S.B., Hussein, S.A., Muhammad, F.F., Yahya, M.Y.: The study of structural and optical properties of PVA:PbO_2 based solid polymer nanocomposites. J. Mater. Sci. Mater. Electron. **27**, 12112–12118 (2016). https://doi.org/10.1007/s10854-016-5363-y

Ahmed, R.M.: Optical study on poly(methyl methacrylate)/poly(vinyl acetate) blends. Int. J. Photoenergy. 2009, **150389** (2009). https://doi.org/10.1155/2009/150389

Ahmed, R.M.: Study on different solution-cast films of PMMA and PVAc. Int. J. Polym. Mater. Polym. Biomater.polym. Mater. Polym. Biomater. **57**, 969–978 (2010). https://doi.org/10.1080/00914030802177396

Ahmed, R.M.: Optical properties and structure of cobalt chloride doped PVA and its blend with PVP. Int. J. Mod. Phys. B **28**, 1450036 (2014). https://doi.org/10.1142/S0217979214500362

Ahmed, R.M.: Surface and spectroscopic properties of CdSe/ZnS/PVC nanocomposites. Polym. Compos.. Compos. **38**, 749–758 (2017). https://doi.org/10.1002/PC.23634

Ahmed, R.M., Ibrahim, A.A., El-Said, E.A.: Enhancing the optical properties of polyvinyl alcohol by blending it with polyethylene glycol. Acta Phys. Pol. A **137**, 317–323 (2020a). https://doi.org/10.12693/APhysPolA.137.317

Ahmed, R.M., Ibrahiem, A.A., El-Said, E.A.: Effect of cobalt chloride as filler and PVP on the optical properties of PVA/PEG/PVP blends. Opt. Spectrosc.spectrosc. **128**, 642–655 (2020b). https://doi.org/10.1134/S0030400X20050033/FIGURES/10

Ahmed, R.M., Soliman, T.S., Vshivkov, S.A., Khalid, A.: Influence of Fe_2O_3@reduced graphene oxide nanocomposite on the structural, morphological, and optical features of the polyvinyl alcohol films for optoelectronic applications. Phys. Scr. **98**, 055928 (2023). https://doi.org/10.1088/1402-4896/accb15

Al-Bataineh, Q.M., Alsaad, A.M., Ahmad, A.A., Telfah, A.: A novel optical model of the experimental transmission spectra of nanocomposite PVC-PS hybrid thin films doped with silica nanoparticles. Heliyon. **6**, e04177 (2020). https://doi.org/10.1016/J.HELIYON.2020.E04177

Ali, F.M.: Structural and optical characterization of [(PVA:PVP)-$Cu2^{+}$] composite films for promising semiconducting polymer devices. J. Mol. Struct.struct. **1189**, 352–359 (2019). https://doi.org/10.1016/J.MOLSTRUC.2019.04.014

Ali, F.M.: Synthesis and characterization of a novel erbium doped poly(vinyl alcohol) films for multifunctional optical materials. J. Inorg. Organomet. Polym. Mater.inorg. Organomet. Polym. Mater. **30**, 2418–2429 (2020). https://doi.org/10.1007/s10904-019-01386-8

Ali, H.E., Khairy, Y.: Optical and electrical performance of copper chloride doped polyvinyl alcohol for optical limiter and polymeric varistor devices. Phys. B Condens. Matter. **572**, 256–265 (2019). https://doi.org/10.1016/j.physb.2019.08.014

Ali, H.E., Morad, I., Algarni, H., El-Desoky, M.M., Khairy, Y., Zahran, H.Y., Yahia, I.S.: Structure analysis and nonlinear/linear optical properties of PVAOH/Si composites for low-cost optical technologies and limiting absorption. J. Mater. Sci. Mater. Electron. **32**, 4466–4479 (2021). https://doi.org/10.1007/S10854-020-05188-4/FIGURES/13

Anani, M., Mathieu, C., Lebid, S., Amar, Y., Chama, Z., Abid, H.: Model for calculating the refractive index of a III-V semiconductor. Comput. Mater. Sci.. Mater. Sci. **41**, 570–575 (2008). https://doi.org/10.1016/j.commatsci.2007.05.023

Aslam, M., Kalyar, M.A., Raza, Z.A.: Graphene oxides nanosheets mediation of poly(vinyl alcohol) films in tuning their structural and opto-mechanical attributes. J. Mater. Sci. Mater. Electron. **28**, 13401–13413 (2017). https://doi.org/10.1007/S10854-017-7177-Y/FIGURES/10

Aziz, S.B., Hassan, A.Q., Mohammed, S.J., Karim, W.O., Kadir, M.F.Z., Tajuddin, H.A., Chan, N.N.M.Y.: Structural and optical characteristics of PVA: C-dot composites: tuning the absorption of ultra violet (UV) region. Nanomaterials **9**, 216 (2019). https://doi.org/10.3390/nano9020216

Aziz, S.B., Dannoun, E.M.A., Tahir, D.A., Hussen, S.A., Abdulwahid, R.T., Nofal, M.M., Abdullah, R.M., Hussein, A.M., Brevik, I.: Synthesis of PVA/CeO_2 based nanocomposites with tuned refractive index and reduced absorption edge: structural and optical studies. Materials (basel). **14**, 1570 (2021). https://doi.org/10.3390/ma14061570

Badapanda, T., Senthil, V., Anwar, S., Cavalcante, L.S., Batista, N.C., Longo, E.: Structural and dielectric properties of polyvinyl alcohol/barium zirconium titanate polymer-ceramic composite. Curr. Appl. Phys.. Appl. Phys. **13**, 1490–1495 (2013). https://doi.org/10.1016/j.cap.2013.05.006

Badawi, A., Ahmed, E.M., Mostafa, N.Y., Abdel-Wahab, F., Alomairy, S.E.: Enhancement of the optical and mechanical properties of chitosan using Fe_2O_3 nanoparticles. J. Mater. Sci. Mater. Electron. **28**, 10877–10884 (2017). https://doi.org/10.1007/S10854-017-6866-X/TABLES/2

Badawi, A., Alharthi, S.S., Althobaiti, M.G., Alharbi, A.N.: The effect of iron oxide content on the structural and optical parameters of polyvinyl alcohol/graphene nanocomposite films. J. Vinyl Addit. Technol.addit. Technol. **28**, 235–246 (2022). https://doi.org/10.1002/VNL.21889

Choudhary, S.: Structural, optical, dielectric and electrical properties of (PEO–PVP)–ZnO nanocomposites. J. Phys. Chem. Solids **121**, 196–209 (2018). https://doi.org/10.1016/j.jpcs.2018.05.017

Choudhary, S., Sengwa, R.J.: Investigation on structural and dielectric properties of silica nanoparticles incorporated poly(ethylene oxide)/poly(vinyl pyrrolidone) Blend matrix based nanocomposites. J. Inorg. Organomet. Polym. Mater.inorg. Organomet. Polym. Mater. **29**, 592–607 (2019). https://doi.org/10.1007/s10904-018-1034-1

Das, S., Senapati, S., Alagarasan, D., Varadharajaperumal, S., Ganesan, R., Naik, R.: Enhancement of nonlinear optical parameters upon phase transition in new quaternary Ge20Ag10Te10Se60 films by annealing at various temperatures for optoelectronic applications. J. Alloys Compd. **927**, 167000 (2022). https://doi.org/10.1016/J.JALLCOM.2022.167000

Dimitrov, V., Sakka, S.: Linear and nonlinear optical properties of simple oxides. II. J. Appl. Phys. **79**, 1741–1745 (1996). https://doi.org/10.1063/1.360963

Divya, S., Lims, S.C., Manivannan, M., Robert, R., Jerome Das, S., Jose, M.: Impact of amorphous SiO_2 as shell material on superparamagnetic Fe_3O_4 nanoparticles and investigation of temperature and frequency dependent dielectric properties. J. Alloys Compd. **919**, 165751 (2022). https://doi.org/10.1016/J.JALLCOM.2022.165751

Donya, H., Taha, T.A., Alruwaili, A., Tomsah, I.B.I., Ibrahim, M.: Micro-structure and optical spectroscopy of PVA/iron oxide polymer nanocomposites. J. Mater. Res. Technol. **9**, 9189–9194 (2020). https://doi.org/10.1016/j.jmrt.2020.06.040

El Sayed, A.M., Saber, S.: Structural, optical analysis, and Poole–Frenkel emission in NiO/CMC–PVP: bionanocomposites for optoelectronic applications. J. Phys. Chem. Solids **163**, 110590 (2022). https://doi.org/10.1016/j.jpcs.2022.110590

El Sayed, A.M., El-Sayed, S., Morsi, W.M., Mahrous, S., Hassen, A.: Synthesis, characterization, optical, and dielectric properties of polyvinyl chloride/cadmium oxide nanocomposite films. Polym. Compos.. Compos. **35**, 1842–1851 (2014). https://doi.org/10.1002/PC.22839

El-Khodary, A.: Vibrational, thermal, optical and magnetic investigations of PVA films filled with $FeCl_3$ and $CoCl_2$. Phys. B Condens. Matter **404**, 1287–1294 (2009). https://doi.org/10.1016/J.PHYSB.2008.11.238

Fasasi, A.Y., Osagie, E., Pelemo, D., Obiajunwa, E., Ajenifuja, E., Ajao, J., Osinkolu, G., Makinde, W.O.: Effect of precursor solvents on the optical properties of copper oxide thin films deposited using spray pyrolysis for optoelectronic applications. Am. J. Mater. Synth. Process. **3**, 12–22 (2018). https://doi.org/10.11648/J.AJMSP.20180302.12

Ghanbari, D., Salavati-Niasari, M., Ghasemi-Kooch, M.: A sonochemical method for synthesis of Fe_3O_4 nanoparticles and thermal stable PVA-based magnetic nanocomposite. J. Ind. Eng. Chem. **20**, 3970–3974 (2014). https://doi.org/10.1016/J.JIEC.2013.12.098

Goumri, M., Venturini, J.W., Bakour, A., Khenfouch, M., Baitoul, M.: Tuning the luminescence and optical properties of graphene oxide and reduced graphene oxide functionnalized with PVA. Appl. Phys. A **3**, 1–8 (2016). https://doi.org/10.1007/S00339-016-9725-3

Güneri, E., Kariper, A.: Optical properties of amorphous CuS thin films deposited chemically at different pH values. J. Alloys Compd. **516**, 20–26 (2012). https://doi.org/10.1016/J.JALLCOM.2011.11.054

Habubi, N.F., Mishjil, K.A., Chiad, S.S.: Structural properties and refractive index dispersion of cobalt doped SnO_2 thin films. Indian J. Phys. **87**, 235–239 (2013). https://doi.org/10.1007/S12648-012-0223-Y/FIGURES/5

Hashim, A.: Enhanced structural, optical, and electronic properties of -In_2O_3 and Cr_2O_3 nanoparticles doped polymer blend for flexible electronics and potential applications. J. Inorg. Organomet. Polym. Mater. inorg. Organomet. Polym. Mater. **30**, 3894–3906 (2020). https://doi.org/10.1007/s10904-020-01528-3

Heiba, Z.K., Bakr Mohamed, M., Ahmed, S.I.: Exploring the physical properties of PVA/PEG polymeric material upon doping with nano gadolinium oxide. Alexandria Eng. J. **61**, 3375–3383 (2022). https://doi.org/10.1016/J.AEJ.2021.08.051

Hervé, P., Vandamme, L.K.J.: General relation between refractive index and energy gap in semiconductors. Infrared Phys. Technol. **35**, 609–615 (1994). https://doi.org/10.1016/1350-4495(94)90026-4

Ismail, M.S., Elamin, A.A., Abdel-Wahab, F., Elbashar, Y.H., Mahasen, M.M.: Improving the refractive index by engineering PbS/PVA nano polymer composite for optoelectronic applications. Opt. Mater. **131**, 112639 (2022). https://doi.org/10.1016/J.OPTMAT.2022.112639

Jannah, M.A., Taufiq, A., Hidayat, N., Usdiana, E.N., Sunaryono, Lestari, N.A.G., Fuad, A., Sugiharto, T.I.: Preparation and structural characterization of nanosized PVA/Fe_3O_4 fibers. J. Phys. Conf. Ser. **1093**, 012040 (2017). https://doi.org/10.1088/1742-6596/1093/1/012040

Jebur, Q.M., Hashim, A., Habeeb, M.A.: Fabrication, structural and optical properties for (polyvinyl alcohol-polyethylene oxide-iron oxide) nanocomposites. Egypt. J. Chem. **63**, 611–623 (2020). https://doi.org/10.21608/ejchem.2019.10197.16696

Kang, H.J.H., Ali, R.F., Paul, M.T.Y., Radford, M.J., Andreu, I., Lee, A.W.H., Gates, B.D.: Tunable functionalization of silica coated iron oxide nanoparticles achieved through a silanol–alcohol condensation reaction. Chem. Commun.commun. **55**, 10452–10455 (2019). https://doi.org/10.1039/C9CC03969D

Khalid, A., Ahmed, R.M., Taha, M., Soliman, T.S.: Fe_3O_4 nanoparticles and Fe_3O_4@SiO_2 core-shell_synthesize, structural, morphological, linear, and nonlinear optical properties. J. Alloys Compd. **947**, 169639 (2023). https://doi.org/10.1016/j.jallcom.2023.169639

Khalil, R., Kelany, N.A., Ibrahim, M.A., Al-senani, G.M., Mostafa, A.M.: Linear and nonlinear optical properties of PVA : SA blend reinforced by TiO_2 nanoparticles prepared by flower extract of aloe vera for optoelectronic applications. Coatings **13**, 699 (2023). https://doi.org/10.3390/coatings13040699

Kumar, V., Singh, J.K.: Model for calculating the refractive index of different materials. Indian J. Pure Appl. Phys. **48**, 571–574 (2010)

Mahdi, M.A., Al-Ani, S.K.J.: Optical characterization of chemical bath deposition Cd1-xZ xxS thin films. Int. J. Nanoelectron. Mater. **5**, 11–24 (2012)

Mohammed, N.J., Rasheed, Z.S., Hassan, A.S.: Improvement optical properties of PVA/TiO_2 and PVA/ZnO nanocomposites, Al-Mustansiriyah. J. Sci. **29**, 118–123 (2019). https://doi.org/10.23851/mjs.v29i3.629

Moss, T.S.: Relations between the refractive index and energy gap of semiconductors. Phys. Status Solidi **131**, 415–427 (1985). https://doi.org/10.1002/PSSB.2221310202

Moumen, A., Hartiti, B., Comini, E., El Khalidi, Z., Arachchige, H.M.M.M., Fadili, S., Thevenin, P.: Preparation and characterization of nanostructured CuO thin films using spray pyrolysis technique. Superlattices Microstruct. Microstruct. **127**, 2–10 (2019). https://doi.org/10.1016/J.SPMI.2018.06.061

Nabil, M., Horia, F., Fouad, S.S., Negm, S.: Impact of Au nanoparticles on the thermophysicalparameters of Fe_3O_4 nanoparticles for seawater desalination. Opt. Mater. **128**, 112456 (2022). https://doi.org/10.1016/j.optmat.2022.112456

Nangia, R., Shukla, N.K., Sharma, A.: Optical and structural properties of Se80Te15Bi5/PVA nanocomposite films. J. Mol. Struct.struct. **1177**, 323–330 (2019). https://doi.org/10.1016/J.MOLSTRUC.2018.09.080

Nikmah, A., Taufiq, A., Hidayat, A.: Synthesis and Characterization of Fe_3O_4/SiO_2 nanocomposites. IOP Conf. Ser. Earth Environ. Sci. **276**, 0–10 (2019a). https://doi.org/10.1088/1755-1315/276/1/012046

Nikmah, A., Taufiq, A., Hidayat, A.: Synthesis and Characterization of Fe_3O_4/SiO_2 nanocomposites. IOP Conf. Ser. Earth Environ. Sci. **276**, 012046 (2019b). https://doi.org/10.1088/1755-1315/276/1/012046

Parthasarathy, V., Selvi, J., Senthil Kumar, P., Anbarasan, R., Mahalakshmi, S.: Evaluation of mechanical, optical and thermal properties of PVA nanocomposites embedded with Fe_2O_3 nanofillers and the investigation of their thermal decomposition characteristics under non-isothermal heating condition. Polym. Bull.. Bull. **78**, 2191–2210 (2021). https://doi.org/10.1007/S00289-020-03206-3/FIGURES/14

Radoń, A., Drygała, A., Hawełek, Ł, Łukowiec, D.: Structure and optical properties of Fe_3O_4 nanoparticles synthesized by co-precipitation method with different organic modifiers. Mater CharactCharact **131**, 148–156 (2017). https://doi.org/10.1016/j.matchar.2017.06.034

Raja, V., Sarma, A.K., Rao, V.V.R.N.: Optical properties of pure and doped PMMA-CO-P4VPNO polymer films. Mater. Lett. **57**, 4678–4683 (2003). https://doi.org/10.1016/S0167-577X(03)00384-7

Rathod, S.G., Bhajantri, R.F., Ravindrachary, V., Naik, J., Kumar, D.J.M.: High mechanical and pressure sensitive dielectric properties of graphene oxide doped PVA nanocomposites. RSC Adv. **6**, 77977–77986 (2016). https://doi.org/10.1039/C6RA16026C

Ravindra, N.M., Auluck, S., Srivastava, V.K.: On the Penn gap in semiconductors. Phys. Status Solidi **93**, K155–K160 (1979). https://doi.org/10.1002/PSSB.2220930257

Reddy, R.R., NazeerAhammed, Y.: A study on the Moss relation. Infrared Phys. Technol. **36**, 825–830 (1995). https://doi.org/10.1016/1350-4495(95)00008-M

Sabarudin, A., Wahid, R., Nalle, F.C., Shobirin, R.A., Santjojo, D.J.D.H.: Designed structure and magnetic characteristic studies of magnetic iron oxide (Fe_3O_4) nanoparticles coated by polyvinyl alcohol and polyvinyl alcohol-linked with glutaraldehyde. Rasayan J. Chem. J. Chem. **10**, 1261–1270 (2017). https://doi.org/10.7324/RJC.2017.1041906

Sajid, M., Shuja, S., Rong, H., Zhang, J.: Size-controlled synthesis of Fe_3O_4 and $Fe_3O_4@SiO_2$ nanoparticles and their superparamagnetic properties tailoring. Prog. Nat. Sci. Mater. Int. **33**, 116–119 (2023). https://doi.org/10.1016/j.pnsc.2022.08.003

Sarkar, S., Das, N.S., Chattopadhyay, K.K.: Optical constants, dispersion energy parameters and dielectric properties of ultra-smooth nanocrystalline $BiVO_4$ thin films prepared by rf-magnetron sputtering. Solid State Sci. **33**, 58–66 (2014). https://doi.org/10.1016/J.SOLIDSTATESCIENCES.2014.04.008

Selvi, J., Mahalakshmi, S., Parthasarathy, V., Hu, C., Lin, Y.F., Tung, K.L., Anbarasan, R., Annie, A.A.: Optical, thermal, mechanical properties, and non-isothermal degradation kinetic studies on PVA/CuO nanocomposites. Polym. Compos.. Compos. **40**, 3737–3748 (2019). https://doi.org/10.1002/PC.25235

Selvi, J., Parthasarathy, V., Mahalakshmi, S., Anbarasan, R., Daramola, M.O., Senthil Kumar, P.: Optical, electrical, mechanical, and thermal properties and non-isothermal decomposition behavior of poly(vinyl alcohol)–ZnO nanocomposites. Iran. Polym. J.polym. J. **29**, 411–422 (2020). https://doi.org/10.1007/s13726-020-00806-8

Shaalan, N.M., Hanafy, T.A., Rashad, M.: Dual optical properties of NiO-doped PVA nanocomposite films. Opt. Mater. **119**, 111325 (2021). https://doi.org/10.1016/J.OPTMAT.2021.111325

Shehap, A.M., Akil, D.S.: Structural and optical properties of TiO_2 nanoparticles/PVA for different composites thin films. Int. J. Nanoelectron. Mater. **9**, 17–36 (2016)

Silva, V.A.J., Andrade, P.L., Silva, M.P.C., Bustamante, A.D., Valladares, L.D.L.S., Aguiar, J.A.: Synthesis and characterization of Fe_3O_4 nanoparticles coated with fucan polysaccharides. J. Magn. Magn. Mater. magn. Magn. Mater. **343**, 138–143 (2013). https://doi.org/10.1016/j.jmmm.2013.04.062

Siva, V., Murugan, A., Shameem, A., Thangarasu, S., Bahadur, S.A.: A facile microwave-assisted combustion synthesis of $NiCoFe_2O_4$ anchored polymer nanocomposites as an efficient electrode material for asymmetric supercapacitor application. J. Energy Storage **48**, 103965 (2022). https://doi.org/10.1016/j.est.2022.103965

Skettrup, T.: Urbach's rule derived from thermal fluctuations in the band-gap energy. Phys. Rev. B **18**, 2622 (1978). https://doi.org/10.1103/PhysRevB.18.2622

Soliman, T.S., Vshivkov, S.A.: Effect of Fe nanoparticles on the structure and optical properties of polyvinyl alcohol nanocomposite films. J. Non Cryst. Solidscryst. Solids **519**, 119452 (2019). https://doi.org/10.1016/j.jnoncrysol.2019.05.028

Soliman, T.S., Vshivkov, S.A., Elkalashy, S.I.: Structural, thermal, and linear optical properties of SiO_2 nanoparticles dispersed in polyvinyl alcohol nanocomposite films. Polym. Compos.. Compos. **41**, 3340–3350 (2020). https://doi.org/10.1002/pc.25623

Somesh, T.E., Al Gunaid, M.Q.A., Siddaramaiah, B.S.M.: Photosensitization of optical band gap modified polyvinyl alcohol films with hybrid—$AgAlO_2$ nanoparticles. J. Mater. Sci. Mater. Electron. **30**, 37–49 (2019). https://doi.org/10.1007/s10854-018-0226-3

Sugumaran, S., Bellan, C.S., Nadimuthu, M.: Characterization of composite PVA–Al_2O_3 thin films prepared by dip coating method. Iran. Polym. J.polym. J. **24**, 63–74 (2015). https://doi.org/10.1007/S13726-014-0300-5/TABLES/4

Suma, G.R., Subramani, N.K., Shilpa, K.N., Sachhidananda, S., Satyanarayana, S.V., Siddaramaiah: Effect of $Ce_{0.5}Zr_{0.5}O_2$ nano fillers on structural and optical behaviors of poly(vinyl alcohol). J. Mater. Sci. Mater. Electron. **28**, 10707–10714 (2017). https://doi.org/10.1007/s10854-017-6846-1

Tichá, H., Tichý, L.: Semiempirical relation between non-linear susceptibility (refractive index), linear refractive index and optical gap and its application to amorphous chalcogenides. J. Optoelectron. Adv. Mater.optoelectron. Adv. Mater. **4**, 381–386 (2002)

Tripathy, S.K.: Refractive indices of semiconductors from energy gaps. Opt. Mater. **46**, 240–246 (2015). https://doi.org/10.1016/J.OPTMAT.2015.04.026

Wemple, S.H., DiDomenico, M.: Behavior of the electronic dielectric constant in covalent and ionic materials. Phys. Rev. B **3**, 1338 (1971). https://doi.org/10.1103/PhysRevB.3.1338

Wise, D.L.: Electrical and Optical Polymer Systems Fundamentals: Methods and Applications. CRC Press (1998)

Yadav, P., Sharma, A.: Investigation of optical nonlinearities in Bi-doped Se-Te chalcogenide thin films. J. Electron. Mater. **44**, 916–921 (2015). https://doi.org/10.1007/S11664-014-3577-4/METRICS

Zhu, Y.S., Wang, X.J., Hou, Y.Y., Gao, X.W., Liu, L.L., Wu, Y.P., Shimizu, M.: A new single-ion polymer electrolyte based on polyvinyl alcohol for lithium ion batteries. Electrochim. Acta. Acta **87**, 113–118 (2013). https://doi.org/10.1016/j.electacta.2012.08.114